Some aspects of the dynamics of active filament solutions

2005 J. Phys.: Condens. Matter 17 S1153

(http://iopscience.iop.org/0953-8984/17/14/003)

INSTITUTE OF PHYSICS PUBLISHING JOURNAL OF PHYSICS: CONDENSED MATTER

J. Phys.: Condens. Matter **17** (2005) S1153–S1163 doi:10.1088/0953-8984/17/14/003

Some aspects of the dynamics of active filament solutions

Tanniemola B Liverpool

Department of Applied Mathematics, University of Leeds, Leeds LS2 9JT, UK

Received 30 August 2004, in final form 8 November 2004
Published 24 March 2005
Online at stacks.iop.org/JPhysCM/17/S1153

Abstract

We study the dynamics of an isotropic solution of polar filaments coupled by molecular motors acting as *active cross-links* which generate relative motion of the filaments in two and three dimensions. We investigate the mechanical properties of the homogeneous and isotropic state. We also consider the stability of the homogeneous state for constant motor concentration, taking into account excluded volume and an estimate of entanglement.

(Some figures in this article are in colour only in the electronic version)

1. Introduction

Soft active systems are a new and exciting class of complex fluids to which energy is continuously supplied by internal or external sources. Biology provides many examples of such systems, including cell membranes and biopolymer solutions driven by chemical reactions, living cells moving on a substrate, and the cytoskeleton of eukariotic cells [1]. The cytoskeleton is a complex network of long filamentary proteins (mainly F-actin and microtubules) cross-linked by a variety of smaller proteins [1, 2]. Among the latter are clusters of motor proteins, such as myosin and kinesin, that use chemical energy from the hydrolysis of ATP to 'walk' along the filaments, mediating the exchange of forces between them [3–6]. This out of equilibrium chemical activity in motor–filament solutions is known to lead to complex cooperative behaviour [4, 7–9] including pattern formation and creation of dissipative structures. In addition, even in the *absence* of macroscopic patterning the mechanical response functions of such a mixture are strongly modified by the novel microscopic dynamics occurring due to the addition of motors to a solution of semiflexible filaments. In this paper we will describe some recent work [10–12] attempting to study certain aspects of these motor–filament systems.

In the next section we consider the linear viscoelastic response of an isotropic solution of entangled polar filaments interacting with motor clusters in the regime where the motors do not lead to the formation of macroscopic patterns. In section 3 using a hydrodynamic approach, we investigate the stability of the isotropic state to the formation of ordered states or patterns.

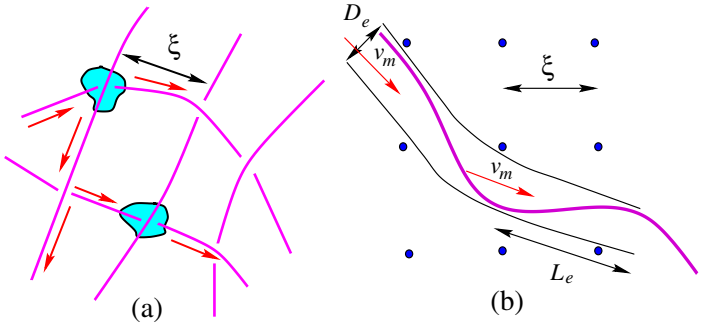

Figure 1. (a) The active solution with motor centres and entanglement points. (b) The 'tube' encircling the polymer and the directed motion $v_{\rm m}$. We show the lengths ξ, $L_{\rm e}$, $D_{\rm e}$.

Finally in section 4 we discuss a microscopic model of the filament–motor interaction enabling us to derive the parameters of the hydrodynamic model.

2. Viscoelastic response of isotropic solutions

An example of a filament/motor mixture is the F-actin-myosin-II system. Myosin spontaneously aggregates *in vitro* to form clusters. In an ATP rich system these myosin clusters can then bind to pairs of filaments and actively move the filaments with respect to each other (see figure 1). In a sheared sample this results in rapid release of elastic strains, for the directed motion of the polymers leads to a reduction of the reptation time from $t_{\rm rept} \sim L^3$ (characteristic of diffusion) to $t_{\rm rept} \sim L$ for filaments of length L sliding at constant speed [6, 13]. Motivated by experimental observations and this simple argument, one is led to ask a number of further *quantitative* questions. What is the elastic stress supported by such a system? What are the relevant relaxation mechanisms and timescales? As a step in this direction, we focus here on a simple model for the viscoelasticity of an 'active' solution of motile semiflexible filaments, within the 'tube' picture of polymer dynamics. This is clearly an over-simplification of the *in vitro* system described above; nevertheless, the physics of the problem, even with this approximation, is interesting and non-trivial.

We consider a monodisperse solution of semiflexible and polar polymers of persistence length $L_{\rm p}$, length L and diameter a, with $L_{\rm p} \gg a$, at a monomer concentration ρ_a such that the mesh-size of the solution, is $\xi \simeq (\rho_a a)^{-1/2} \ll L_{\rm p}, L$ [14]. We model the ATP induced activity of actin clusters by stochastic forces on the polymers, *parallel to the filament contour* (transverse motion is constrained by entanglements), which always act in the same direction with respect to the polarity of the filaments. The effect of the motor activity is

(1) to increase the amplitude of the *longitudinal* fluctuations along the contour of the filaments giving rise to a higher *effective* temperature $T \to T + T_{\rm act}$ for the tangential motion, and
(2) to give the filaments a non-zero curvilinear drift velocity in their tubes, $v_{\rm m}$.

Increasing/decreasing activity leads to an increase/decrease in $T_{\rm act}$ and $v_{\rm m}$. A sketch of the system is shown in figure 1. Effective temperatures for non-equilibrium systems have been used to model noise in foams and other driven systems [15].

We derive the linear viscoelastic response of such an *active* polymer solution, assuming that its structure is not perturbed by the activity of the motor clusters. This is a very crude assumption; nevertheless, we uncover rich physical behaviour, as the 'activity' modifies the already subtle dynamics of *passive* semiflexible polymer solutions [19–23].

The linear response of this active filament solution to a weak time dependent shear strain, $\gamma_{ij}(t)$, is characterized by the shear modulus $G(t)$, such that the shear stress is [14]

$$\sigma_{ij}(t) = \int_{-\infty}^{t} \mathrm{d}t'\, G(t-t')\dot{\gamma}_{ij}(t'). \tag{1}$$

The shear modulus can be most simply be calculated by calculating the stress due to the application of a step strain for which $\dot{\gamma}(t) = \gamma\delta(t)$.

The stress is calculated from the fluctuating dynamics of Kratky–Porod worm-like chains. A *typical* filament conformation is parameterized by $\mathbf{R}(s)$. The Hamiltonian of a worm-like chain is given by

$$\mathcal{H}_{\mathrm{wlc}}[\mathbf{R}(s), \Lambda(s)] = \kappa/2 \int_0^{\mathrm{L}} \mathrm{d}s\, |\partial_{\mathrm{s}}^2\mathbf{R}|^2 + \int_0^{\mathrm{L}} \mathrm{d}s\, \Lambda(s)(|\partial_{\mathrm{s}}\mathbf{R}|^2 - 1), \tag{2}$$

where $\partial_x A \equiv \partial A/\partial x$ and an instantaneous local tension, $\Lambda(s)$, is induced by the incompressibility of the chain. The persistence length $L_{\mathrm{p}} = \kappa/k_{\mathrm{B}}T$ is the length scale over which the chain loses memory of its orientation. The filaments are confined to a 'tube' [14] of diameter $D_{\mathrm{e}} \sim L_{\mathrm{p}}(\xi/L_{\mathrm{p}})^{6/5}$. We define an entanglement (deflection) length [16, 18] $L_{\mathrm{e}} \sim L_{\mathrm{p}}(\xi/L_{\mathrm{p}})^{4/5}$, the distance between successive collisions of the filament with its tube (see figure 1(b)). The hierarchy of length scales is $L, L_{\mathrm{p}} \gg L_{\mathrm{e}} \gg a$. On length scales ℓ less than L_{e}, the relaxation is due to the dynamics of 'free' chains [14], whilst for $\ell > L_{\mathrm{e}}$ it is due to diffusive directed motion of the polar filaments in their tubes. For $\ell < L_{\mathrm{e}}$ (and consequently $\ell < L_{\mathrm{p}}$), the chain conformation is anisotropic and can be described by an expansion about a rod with orientation $\hat{\mathbf{u}}$ (a unit vector, $|\hat{\mathbf{u}}|^2 = 1$), $\mathbf{R}(s,t) = (s - r_{\parallel}(s,t))\hat{\mathbf{u}} + \mathbf{r}_{\perp}(s,t)$; $\hat{\mathbf{u}}\cdot\mathbf{r}_{\perp}(s,t) \equiv 0$ with parallel (longitudinal) and perpendicular (transverse) components of motion, $r_{\parallel}$, $|\mathbf{r}_{\perp}| \ll s$. The filament dynamics in a shear flow are described by the equations [25],

$$\begin{aligned}\partial_t \mathbf{r}_{\perp}(s,t) = \zeta_{\perp}^{-1}\left[-\kappa\partial_{\mathrm{s}}^4\mathbf{r}_{\perp} + \Lambda(s,t)\partial_{\mathrm{s}}^2\mathbf{r}_{\perp} + \partial_{\mathrm{s}}\Lambda\partial_{\mathrm{s}}\mathbf{r}_{\perp} + \boldsymbol{f}_{\perp}(s,t)\right] \\ + (\mathbf{I} - \hat{\mathbf{u}}\hat{\mathbf{u}})\cdot\dot{\boldsymbol{\gamma}}(t)\cdot\mathbf{r}_{\perp} + \mathrm{O}(|\partial_{\mathrm{s}}\mathbf{r}_{\perp}|^3)\end{aligned} \tag{3}$$

$$\partial_t r_{\parallel}(s,t) = \zeta_{\parallel}^{-1}\left[-\kappa\partial_{\mathrm{s}}^4 r_{\parallel} - \partial_{\mathrm{s}}\Lambda + f_{\mathrm{m}}(s,t) + f_{\parallel}(s,t)\right] + \dot{\gamma}_{ij}(t)\hat{u}_i\hat{u}_j(r_{\parallel} - s) + \mathrm{O}(|\partial_{\mathrm{s}}\mathbf{r}_{\perp}|^3). \tag{4}$$

Due to the constraint of constant length,

$$\partial_{\mathrm{s}} r_{\parallel} = \tfrac{1}{2}|\partial_{\mathrm{s}}\mathbf{r}_{\perp}|^2 + \mathrm{O}(|\partial_{\mathrm{s}}\mathbf{r}_{\perp}|^4), \tag{5}$$

which determines Λ, equations (3), (4) are coupled. Because of the rod-like nature of the polymer segment, the coupling to the shear flow is anisotropic. The friction coefficients are $\zeta_{\parallel} = 2\pi\eta\log|\xi/a| = \frac{1}{2}\zeta_{\perp}$. For short filaments $L < L_{\mathrm{p}}$, the rotational diffusion of a rod of length L determines the dynamics of $\hat{\mathbf{u}}(t)$ which is much slower than that of $r_{\parallel}, \mathbf{r}_{\perp}$. We have in addition to the thermal fluctuating force ($f_{\parallel}(s,t)$, $\boldsymbol{f}_{\perp}(s,t)$) a *non-equilibrium* or *active* force, $f_{\mathrm{m}}(s,t)$, in the *longitudinal* direction due to the activity of the motors. The thermal force has zero mean, $\langle \boldsymbol{f}(s,t)\rangle = 0$, and mean square fluctuations $\langle f_i(s,t) f_j(s',t')\rangle = 2k_{\mathrm{B}}T\delta_{ij}\zeta_i\delta(s-s')\delta(t-t')$, where the subscripts $\{i\}$ refer to $\parallel, \perp$. We choose to model the active force by a non-zero mean $\langle f_{\mathrm{m}}(s,t)\rangle = \zeta_{\parallel}v_{\mathrm{m}}$ and mean square fluctuations of the form $\delta f_{\mathrm{m}}(s,t) = f_{\mathrm{m}}(s,t) - \langle f_{\mathrm{m}}(s,t)\rangle$, $\langle \delta f_{\mathrm{m}}(s,t)\delta f_{\mathrm{m}}(s',t')\rangle = 2k_{\mathrm{B}}T_{\mathrm{act}}\zeta_{\parallel}\delta(s-s')\delta(t-t')$, giving an active contribution, T_{act}, to the 'temperature' of the longitudinal motion. A self-consistent description [24, 25] of the dynamics can be obtained from the solution of equations (3), (4) and inextensibility. Because the transverse dynamics is cut off at L_{e}, there is different behaviour at high and low frequencies with a cross-over frequency $\omega_{\mathrm{e}} = 2\alpha\pi/L_{\mathrm{e}}^4$ ($\alpha = \kappa/\zeta_{\perp}$). The dynamic fluctuations of semiflexible filaments are anisotropic [24, 25]. After time t, longitudinal fluctuations are relaxed over a length $\ell_{\parallel}(t) = (tk_{\mathrm{B}}T(2L_{\mathrm{p}})^5/2\pi\eta)^{1/8}$ for $t < 1/\omega_{\mathrm{e}}$

and $\ell_\parallel(t) = (tk_BTL_p^2L_e^{-3}/2\pi\eta)^{1/2}$ for $t > 1/\omega_e$. In comparison, transverse fluctuations are relaxed over a length $\ell_\perp(t) = (tk_BTL_p/4\pi\eta)^{1/4}$ for $t < 1/\omega_e$ [25] and can only relax by reptation for $t > 1/\omega_e$.

We calculate the Kramers–Kirkwood stress tensor [14],

$$\boldsymbol{\sigma}_{ij}(t) = -\frac{\rho_a}{\ell}\int_0^\ell \mathrm{d}s\,\langle F_i(s,t)R_j(s,t)\rangle, \tag{6}$$

where $\mathbf{F}(s,t)$ is the *total* force on the filament at arc-length s at time t, and $\mathbf{R}(s,t) = (s - r_\parallel)\hat{\mathbf{u}} + \mathbf{r}_\perp$ is the position of the filament. The force balance equations (3), (4) and the rotational dynamics give $\mathbf{F}(s,t)$. After subtracting the minor contributions and the isotropic part of the stress, we obtain

$$\boldsymbol{\sigma}_{ij}(t) \simeq \left\langle \frac{\rho_a}{\ell}\int_0^{\ell\sim L_p} \mathrm{d}s \left\{ \hat{u}_i\hat{u}_j \Big(\underbrace{s\partial_s\Lambda}_{\sigma^{(1)}} - \underbrace{r_\parallel\partial_s\Lambda}_{\sigma^{(2)}} \Big) - \underbrace{\kappa\partial_s^4 r_{\perp i}r_{\perp j} + \partial_s\left(\Lambda\partial_s r_{\perp i}\right)r_{\perp j}}_{\sigma^{(3)}} \right\} + \underbrace{3\frac{\rho_a a}{L}k_BT\left(\hat{u}_i\hat{u}_j - \frac{1}{3}\delta_{ij}\right)}_{\sigma^{(4)}} \right\rangle, \tag{7}$$

where the average is over thermal and active fluctuations and orientation. Three of the four contributions to the shear stress, $\sigma_{ij}^{(1,3,4)}$, arise from the coupling of the strain to $r_\parallel$, $\mathbf{r}_\perp$ and $\hat{\mathbf{u}}$, respectively. They have been analysed recently for *passive* solutions [19–23], and named tension, curvature and orientational stress, respectively. The term $\sigma_{ij}^{(2)} = -\langle\frac{\rho_a}{\ell}\int_0^{\ell\sim L_p}\mathrm{d}s\, r_\parallel\partial_s\Lambda\rangle$, which we call the *longitudinal* stress, is new. It has been ignored in passive polymer solutions, $T_{act} = 0$, for it is then much smaller than the other three. In active polymer solutions, however, for large enough motor activity, i.e. $T_{act}/T > (L_p/L_e)^{5/2} - 1$, it can dominate the high-frequency response.

The short-time (high-frequency) moduli as well as terminal relaxation times differ from those of passive polymer solutions. The *active* solution is harder at high frequencies due to the increased fluctuations of the longitudinal modes. These *also* change the relative magnitude of the longitudinal and transverse fluctuations, leading to two new relaxation regimes. At very low frequencies, the directed motion of the filaments leads to a softening or fluidification as suggested in the introduction. Our results are shown schematically in figure 2 and summarized as follows. Upon submitting the system to a step shear, the shear modulus $G(t)$ decays for very short times as $t^{-3/4}$, as for passive polymer solutions [22, 23]. This holds up to a time $t_0 \sim (1 + T_{act}/T)^{-8/5}L_p^3\eta/k_BT$, where we find a regime with two new power law decays: $G(t) \sim t^{-1/8}$ up to a time $t_1 \sim \eta L_p^{-1/5}\xi^{16/5}/k_BT$ and a modulus $G_2 \sim k_B(T + T_{act})\xi^{-12/5}L_p^{-3/5}$, after which there is a faster decay $G(t) \sim t^{-1/2}$ (η is the solvent viscosity). In the long-time regime, the relaxation modulus develops a plateau, as *trapped* stress cannot relax due to entanglements before the filaments escape from their initial tubes [14]. Whilst the magnitude of the plateaus are the same as for passive polymer solutions, the tube renewal time has a different dependence on chain length L and persistence length L_p. When $L/L_p \gg 1$, the dominant stress is due to constrained transverse fluctuations of the filament [19, 20, 22] leading to a plateau of magnitude $G_3 \sim \xi^{-14/5}k_BT/L_p^{1/5}$ which begins at a time $t_2^{coil} \sim L_p^3(\xi/L_p)^4(1+T_{act}/T)^2\eta/k_BT$, and decays after a time $t_3 \simeq L/v_m$. For filaments with $L/L_p \ll 1$, the stress is due to constrained orientational dynamics [16–18, 22], and from $t_2^{rod} \sim L^2L_p(\xi/L_p)^{12/5}(1+T_{act}/T)^2\eta/k_BT$ we find a plateau of magnitude $G_4 \sim k_BT\xi^{-2}L^{-1}$ which decays after a time $t_4 \simeq \sqrt{LL_p}/v_m$.

We estimate typical timescales and moduli from a direct mapping of our calculation onto the F-actin/myosin-II system. We have modelled the noise as a Gaussian white-noise of non-

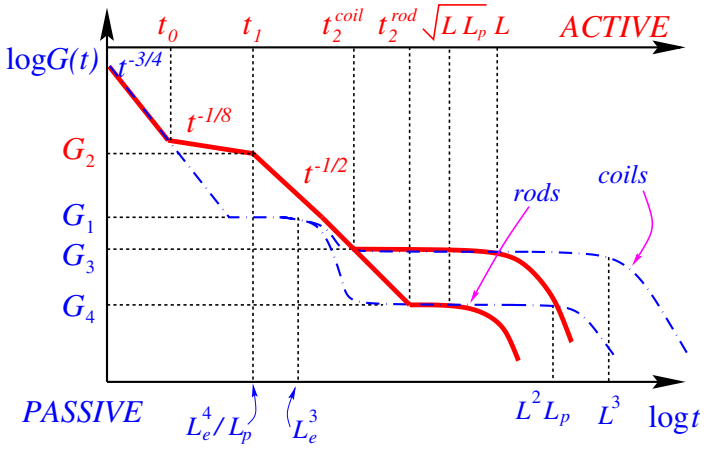

Figure 2. Shear modulus as a function of time t: comparison of active (thick-solid) and passive (thin-dashed) solutions. The different regimes separated by t_0, t_1, $t_2^{\rm coil}$, $t_2^{\rm rod}$, t_3 and t_4, respectively. Top: timescale for active solutions. Bottom: timescale for passive solutions.

zero mean. In a slightly more realistic picture, a motor centre has periods of activity of duration $t_{\rm s}$ (the power-stroke) during which a constant force f_0 is applied, separated by passive periods which are Poisson distributed with a mean duration $\alpha t_{\rm s}$; $\alpha \gg 1$. The motor clusters are also assumed to be randomly distributed along the filaments at a mean distance $\ell_{\rm m}$. Assuming that clusters act independently, we estimate from the mean force $v_{\rm m} \simeq (1+\alpha)^{-1} f_0/\zeta_\parallel \ell_{\rm m}$, and from the local fluctuations of the force about its mean $k_{\rm B}T_{\rm act} \simeq f_0^2 t_{\rm s}\alpha/(1+\alpha)\zeta_\parallel \ell_{\rm m}$. If myosin is at a concentration $\rho_{\rm m}$ and the mean number of myosin per cluster is N, then $\ell_{\rm m} \sim N(\rho_{\rm m}\xi^2)^{-1}$. Let us turn to numbers: a bound myosin has a power stroke of duration $t_{\rm s} \simeq 5$ ms, a step size of $d_{\rm s} \simeq 10$ nm, and a stall force of $f_{\rm max} \simeq 4$ pN [1]. By considering viscous drag, we estimate $f_0 \simeq 0.1$ pN $\ll f_{\rm max}$. Actin has persistence length $L_{\rm p} \simeq 17\ \mu$m and diameter $a \simeq 7$ nm. A solution of F-actin at a typical concentration 100 μg ml^{-1} has a mesh size $\xi \sim 0.5\ \mu$m. For $\rho_{\rm m} = 0.1\ \mu$M (micromolar) and $N \simeq 10$ we estimate $\ell_{\rm m} \sim 5\ \mu$m. This gives $T_{\rm act}/T \sim 10^2$, so that the high-frequency behaviour described above should be relevant. The cross-over modulus between the high and intermediate frequency regimes is $G_2 \sim 10$ Pa. Long-time *fluidification* is also clear: relaxation times for coils ($L = 50\ \mu$m) and rod-like polymers ($L = 5\mu$m) are respectively $t_3 \sim 1$ s and $t_4 \sim 0.1$ s, compared to $t_3 \sim 10^4$ s and $t_4 \sim 100$ s for passive solutions at the same actin concentration. The corresponding plateaus are respectively $G_3 \sim 10^{-2}$ Pa and $G_4 \sim 10^{-4}$ Pa.

3. Instabilities of the isotropic state

In the previous section we considered the situation in which the active solution (like a solution of passive polymers) had an homogeneous and isotropic steady state. In other words, the addition of motors to the passive solution did not lead to any ordered states or to the formation of macroscopic patterns, including radial arrays or asters and one-dimensional bundles. It has been shown both experimentally and theoretically [4, 7, 9] that dissipative structures can be formed by filament/motor mixtures. It is therefore interesting to consider the conditions under which such an isotropic state of our system of polar filaments with *active cross-links* (see figure 1) is stable, and hence for which the arguments of the previous section are valid.

Continuum models of active filament systems have been used to show that spatial patterns are obtained as non-equilibrium solutions of the system dynamics [26, 27, 30–32]. Such hydrodynamic models use symmetry arguments to propose the dynamics of coarse-grained fields for density and polarization of filaments. A more microscopic but still phenomenological approach was taken by Kruse and Jülicher [9, 33], who starting with a model for the relative velocity between filaments considered a dynamical model for the development of contractile and motile structures in polar filament bundles.

We would like therefore to make a connection between the hydrodynamic picture and more microscopic models. As a step in this direction, we start from a phenomenological model in the spirit of Kruse *et al* [9, 33] and obtain a set of continuum equations to describe the dynamics and organization of polar filaments driven by molecular motors in an unconfined geometry in (quasi-)two and three dimensions ($d = 2, 3$).[1] By modelling the motor–filament interaction microscopically, we can determine the magnitude and, most importantly, the sign of the parameters of the continuum equations, which cannot be obtained by symmetry arguments. We consider a isotropic filament solution, include *excluded volume* and estimate the effects of *entanglement* on the diffusive dynamics. Our result is a phase diagram (figure 4) as a function of the filament density and motor properties that is expected to be relevant to the analysis of recent experiments [5].

The filaments are modelled as rigid rods of length l and diameter $b \ll l$. Each filament is identified by the position $\mathbf{r}$ of its centre of mass and a unit vector $\hat{\mathbf{u}}$ pointing towards the polar end. Taking into account *filament transport*, the normalized filament probability distribution function, $\Psi(\mathbf{r}, \hat{\mathbf{u}}, t)$, obeys a conservation law [14],

$$\partial_t \Psi + \nabla \cdot \mathbf{J} + \boldsymbol{\mathcal{R}} \cdot \mathbf{J}^{\mathbf{r}} = 0, \tag{8}$$

where $\mathcal{R} = \hat{\mathbf{u}} \times \partial_{\hat{\mathbf{u}}}$ is the rotation operator. The translational and rotational currents $\mathbf{J}$ and $\mathbf{J}^{\mathbf{r}}$ have diffusive terms, contributions coming from excluded volume and active contributions coming from the motors. Following Kruse *et al*, the active contributions are obtained from relative velocities of interacting filaments due to the motors which are parameterized by the parameters α, β and γ, the rates for the various motor-induced translations and rotations (figure 3). The contribution proportional to α depends on the separation of the centres of the filaments and results from a difference in motor activity between the ends and mid-points of the filaments. It tends to align the centres of mass and polar heads of the pair (see figure 3(a)). The contribution proportional to β vanishes for aligned filaments and can separate antiparallel filaments, as illustrated in figure 3(c). This mechanism yields both translational and rotational currents. The γ term tends to rotate filaments until they are parallel or perpendicular.

We focus on the filament dynamics on length scales large compared to their length, l, where the filament dynamics can be described in terms of the filament density $\rho(\mathbf{r})$ and the local filament orientation $\mathbf{p}(\mathbf{r})$ defined as the first two moments of the distribution $\Psi(\mathbf{r}, \hat{\mathbf{u}}, t)$,

$$\begin{pmatrix} \rho(\mathbf{r}, t) \\ \mathbf{p}(\mathbf{r}, t) \end{pmatrix} = \int \mathrm{d}\hat{\mathbf{u}} \begin{pmatrix} 1 \\ \hat{\mathbf{u}} \end{pmatrix} \Psi(\mathbf{r}, \hat{\mathbf{u}}, t). \tag{9}$$

Coarse-grained equations for ρ and $\mathbf{p}$ can be obtained by using the expressions for the active and diffusive (passive) currents, writing the density $\Psi(\mathbf{r}, \hat{\mathbf{u}}, t)$ in the form of an exact moment expansion, and retaining only the first two moments in this expansion [11]. The dynamical equations obtained can be linearized about a homogeneous state, with constant density ρ_0 and an isotropic orientational distribution of filaments, corresponding to $\mathbf{p} = 0$. Letting $\rho = \rho_0 + \delta\rho$

[1] We assume that even in 3d, motors only induce relative displacement and rotation within the plane that contains the two cross-linked filaments.

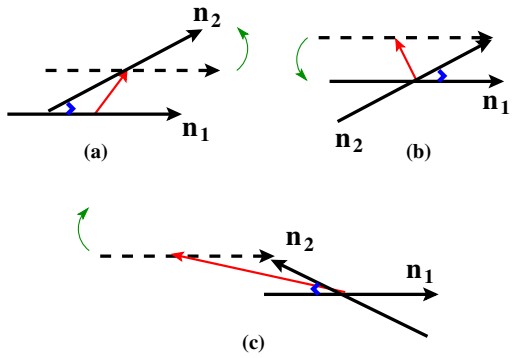

Figure 3. Sketckes of motor-induced filament interactions, viewed from the rest frame of filament 2. The angular bracket connecting each pair of filaments represents the motor. A thick and a dashed arrow show the position of filament 1 before and after translation, respectively. In each case the translation is followed by a rotation at a rate γ in the direction indicated by the curved arrow. (a) The contribution to $\mathbf{v}$ proportional to α is along the direction of the relative displacement $\boldsymbol{\xi}$ of the centres of mass of the two filaments (thin arrow). The contribution to $\mathbf{v}$ proportional to β is illustrated in (b) and (c) for two filaments with $\boldsymbol{\xi} = 0$ and $\hat{\mathbf{n}}_1 \cdot \hat{\mathbf{n}}_2 > 0$ (b) and $\hat{\mathbf{n}}_1 \cdot \hat{\mathbf{n}}_2 < 0$ (c). In both cases the translation at a rate β in the direction of $\hat{\mathbf{n}}_2 - \hat{\mathbf{n}}_1$ (thin arrow) tends to bring the polar heads of the two filaments to the same spatial location. In (b) the counterclockwise rotation aligns the filaments, while in (c) the clockwise rotation anti-aligns and separates them.

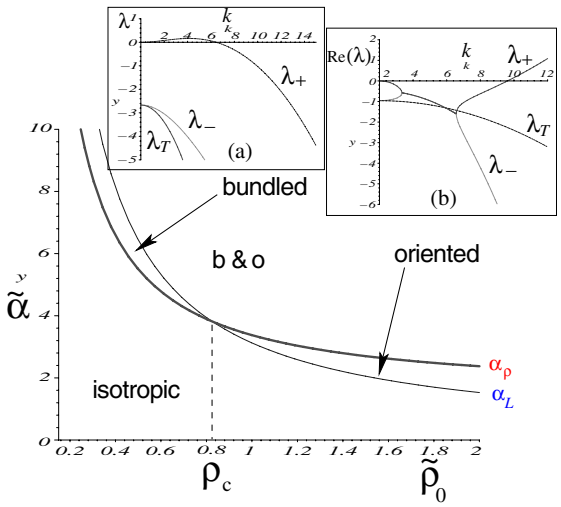

Figure 4. Phase diagram for $\beta = 0$. For $\tilde{\rho}_0 < \rho_c \approx 0.826$ and $\alpha_\rho < \tilde{\alpha} < \alpha_L$, density fluctuations grow on all scales, while orientational fluctuations are stable ('bundled' state). For $\tilde{\rho}_0 < \rho_c$ and $\alpha_L < \tilde{\alpha} < \alpha_\rho$ short scale orientational fluctuations are unstable, while density fluctuations remains stable ('oriented' state). All modes are unstable for $\tilde{\alpha} > \max(\alpha_\rho, \alpha_L)$. The insets show the modes at finite $\tilde{\beta}$ for $\tilde{\alpha} = 5.65$, $\tilde{\beta} = 0.14$, $\tilde{\rho}_0 = 0.5$ (bundled) and $\tilde{\alpha} = 2.3$, $\tilde{\beta} = 0.09$, $\tilde{\rho}_0 = 1.5$ (oriented).

and keeping only terms up to third order in the gradients, the linearized equations are given by

$$\partial_t \delta\rho = \frac{1}{d}\big[D_\parallel + (d-1)D_\perp\big](1 + v_0\rho_0)\nabla^2\delta\rho - \frac{\alpha l v_0 \rho_0}{12d}\nabla^2\delta\rho - \frac{\beta l^2 v_0 \rho_0 (2d+1)}{24d(d+2)}\nabla^2(\boldsymbol{\nabla}\cdot\mathbf{p}), \tag{10}$$

$$\partial_t t_i = -D_r t_i + \frac{1}{d+2}\left[(d+1)D_\perp + D_\parallel\right]\nabla^2 t_i + \frac{2}{d+2}\left(D_\parallel - D_\perp\right)\partial_i \nabla\cdot\mathbf{p} - \frac{\alpha l v_0 \rho_0}{12d(d+2)}\left[\nabla^2 t_i + 2\partial_i \boldsymbol{\nabla}\cdot\mathbf{p}\right] + \frac{\beta v_0 \rho_0}{d}\partial_i \delta\rho + \frac{\beta l^2 v_0 \rho_0 (2d+1)}{24 d^2 (d+2)}\partial_i \nabla^2 \delta\rho, \quad (11)$$

where $D_\perp$, $D_\parallel$ are the transverse and longitudinal diffusion constants and D_r the rotational diffusion constant. The local orientation is not a conserved variable and decays at a rate $\sim D_r$. Both equations display the competition of diffusive terms ($\propto D\nabla^2$) and pattern-forming terms ($\propto -\alpha\nabla^2$). The linear instability of the homogeneous state occurs when the pattern-forming terms dominate. To linear order, the contribution from the rotational current (proportional to γ) vanishes and excluded volume corrections only appear in the density equation.

To study the linear stability of the homogeneous state, we expand the fields in Fourier components, $\delta\rho(\mathbf{r}) = \sum_{\mathbf{k}} \rho_{\mathbf{k}} e^{i\mathbf{k}\cdot\mathbf{r}}$ and $\mathbf{p}(\mathbf{r}) = \sum_{\mathbf{k}} \mathbf{p}_{\mathbf{k}} e^{i\mathbf{k}\cdot\mathbf{r}}$, and separate $\mathbf{p}_{\mathbf{k}}$ into its components longitudinal and transverse to $\mathbf{k}$, namely $p^{\mathrm{L}}_{\mathbf{k}} = \hat{\mathbf{k}}\cdot\mathbf{p}_{\mathbf{k}}$ and $p^{\mathrm{T}}_{\mathbf{k}} = \hat{\mathbf{k}}\times\mathbf{p}_{\mathbf{k}}$, with $\hat{\mathbf{k}} = \mathbf{k}/|\mathbf{k}|$. In d dimensions there are $d-1$ degenerate transverse modes describing the decay of fluctuations in $p^{\mathrm{T}}_{\mathbf{k}}$, with rate $\lambda_T(k)$. There are two coupled modes describing the decay of density and $p^{\mathrm{L}}_{\mathbf{k}}$ fluctuations, given by $\lambda_\pm(k)$. Stability is controlled by the real part of the largest eigenvalue, $\lambda_+(k)$, we need to specify the various diffusion constants. For dilute solutions of long thin rods these are $D_\perp = D_\parallel/2 = D/2$ and $D_r = 6D/l^2$, with $D = k_B T \ln(l/b)/(2\pi\eta l)$ and η the solvent viscosity [14]. At higher density, the dynamics is modified by the topological constraint that the filaments cannot pass through each other, resulting in entanglement. This strongly suppresses transverse and rotational diffusion. Entanglement affects both the diffusive and the active currents. For a first estimate of its role on the dynamics of active solutions, we incorporate its effect only on the diffusive currents and do so by replacing the various diffusion constants by the values obtained in the literature for the corresponding entangled *passive* system, $D_\perp \simeq D/[2(1 + c_\perp \tilde{\rho}_0 (l/b)^{d-2})^2]$ and $D_r \simeq 6D/[l^2(1 + c_r \tilde{\rho}_0 (l/b)^{d-2})^2]$, with $c_{r,\perp}$ constants of order unity and $D_\parallel$ essentially unaffected by entanglement [14, 34].

It is instructive to first consider the case of $\beta = 0$, where the two longitudinal modes are decoupled. The decay rates of density and $p^{\mathrm{L}}_{\mathbf{k}}$ fluctuations are given by λ_ρ and λ_L, respectively. At low density, λ_ρ exceeds λ_L for all k, and becomes positive for $\tilde{\alpha} = \alpha l/(8D) > \alpha_\rho(\tilde{\rho}_0)$ on all length scales, with $\alpha_\rho = (3/2)\left[1 + 1/\tilde{\rho}_0 + 1/(2(1+\tilde{\rho}_0))\right]$, for $d = 2$ ($c_\perp = c_r = 1$). At high density, λ_L exceeds λ_ρ, and orientational fluctuations with $k > k_0 \sim (\tilde{\alpha} - \alpha_L)^{-1/2}\tilde{\rho}_0^{-3/2}$ become unstable for $\tilde{\alpha} > \alpha_L(\tilde{\rho}_0) = (3/\tilde{\rho}_0)\left[1 + (1+\tilde{\rho}_0)^{-2}/2\right]$, while density fluctuations can remain stable. The phase diagram in the $(\tilde{\alpha}, \tilde{\rho}_0)$ plane is shown in figure 4. We define a critical line $\alpha_p(\tilde{\rho}_0)$ as the value of $\tilde{\alpha}$ above which the orientational mode becomes unstable at a $k_0 < 1/l$, with the result $\alpha_p = \tilde{\alpha}_L + 24/(\tilde{\rho}_0(1+\tilde{\rho}_0)^2)$.

A finite value of $\tilde{\beta} = \beta l/(8D)$ has two effects on the structure of the linear modes. First, the modes can change from diffusive at small k to propagating above a typical wavevector $\sim \tilde{\beta}^{-1/2}$, reflecting the oscillatory behaviour arising from the competition between bundling ($\tilde{\alpha}$) and separation ($\tilde{\beta}$). Second, $\tilde{\beta}$ stabilizes the homogeneous state at large length scales. As for $\beta = 0$, at low density the homogeneous state becomes unstable via a *stationary* instability [11]. Consideration of the eigenvector shows that at the largest scales this instability driven by filament bundling ($\tilde{\alpha}$) is associated with density fluctuations. At intermediate scales, where the growth rate is largest, it describes coupled density and orientational fluctuations, suggesting that the 'bundled' state may have a definite orientation on short scales. At high density the behaviour is controlled by an *oscillatory* instability [11], describing the growth of orientational fluctuation. The phase diagram in the $(\tilde{\alpha}, \tilde{\rho}_0)$ plane is similar to that obtained for $\tilde{\beta} = 0$. The instability is driven by α that controls filament bunching, while filament separation

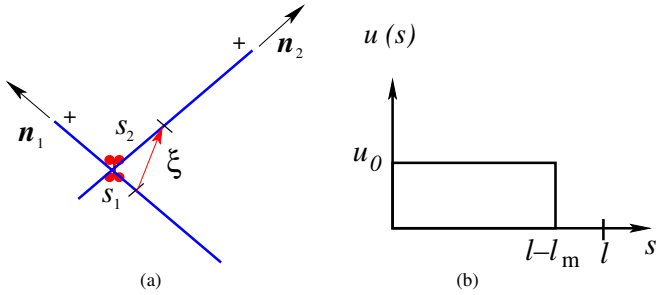

Figure 5. (a) The two filaments connected by an active cross-link and the geometry of the overlap: the filaments' centres are separated by $\boldsymbol{\xi} = s_1\hat{\mathbf{n}}_1 - s_2\hat{\mathbf{n}}_2$. (b) The profile of the motor stepping rate.

driven by terms proportional to β stabilizes the homogeneous state on short length scales. The rotation rate γ plays no role to linear order.

4. Estimating α, β, γ

In the previous section the boundaries of stability of the homogeneous state were calculated in terms of the parameters α, β, γ which characterized the relative velocity of two interacting filaments due to motor activity. In this section we indicate how one can derive the motor-mediated velocities between filaments from a microscopic description of the forces exchanged between the motors and the filaments, thus establishing the connection between the hydrodynamic equations and the microscopic motor dynamics.

Each filament is identified by the location $\mathbf{r}_i$ of its centre of mass and a unit vector $\hat{\mathbf{n}}_i$ pointing towards the polar end. The mobile cross-links are formed by small aggregates of molecular motors that exert a force on filaments by converting chemical energy from the hydrolysis of ATP into mechanical work. Each motor cluster is assumed to be composed of two heads, with the ith head ($i = 1, 2$) attached to filament i at position $\mathbf{r}_i^{\times} = \mathbf{r}_i + \hat{\mathbf{n}}_i s_i$, with s_i the position along the filament relative to the centre of mass, $-l/2 \leqslant s_i \leqslant +l/2$. The motor cluster has size $l_{\mathrm{m}} \ll l$. A schematic is shown in figure 5. Motor heads are assumed to step towards the polar end of filaments at a known speed, $u(s)$, which generally depends on the point of attachment. Spatial variations of $u(s)$ may for instance arise from motors slowing down as they approach the polar end of the filament due to crowding [28]. This is incorporated here by using the step-like speed profile shown in figure 5, where $u(s)$ is constant along the filament, but vanishes in a small region of extent $l_{\mathrm{m}} \ll l$ at the polar end. Both filaments and motors move through a solution. We assume that the filament dynamics is overdamped and the friction of motors is very small compared to that of filaments. Momentum conservation then requires that in the absence of external forces and torques, the total force acting on filaments centred at a given position be balanced by the frictional force experienced by the filament while moving through the fluid. For a small rigid cluster, angular momentum conservation means that we find $\gamma = 0$. We put all these elements together (details of the calculations are given elsewhere [12]) to obtain similar hydrodynamic equations to those obtained from the phenomenological model, but with a number of terms missing and some new terms present [12]. The terms leading to bundling and separation though are easily identified, and allow us to give the estimates

$$\alpha \approx m_0 v_0 u_0 l_{\mathrm{m}}, \tag{12}$$

$$\beta \approx 2 m_0 v_0 u_0. \tag{13}$$

The parameter α has the dimensions of a diffusion constant and describes filament bunching or bundling, which, in contrast to conventional diffusion, tends to enhance density fluctuations. The coefficient β is a velocity and describes the rate at which motor clusters sort or separate filaments of opposite polarity. If the motor stepping speed $u(s)$ is constant, independent of the position s along the filament, then $\alpha = 0$. In general, even when $\alpha \neq 0$, we expect $\alpha \ll \beta$. So we see that for mean-field models of the type considered here a varying motor velocity profile which goes to zero at the + end is required for the formation of inhomogeneous states.

5. Discussion

The rich behaviour of mixtures of filaments and motors is still far from being completely understood. The validity of the simple picture in section 2 needs to be investigated and tested by experiment. Even in the isotropic regime, an active solution could be pre-stressed, and it is possible that imposing a shear flow could decrease rather than increase the stress. Within a tube model we have assumed that the tube has the same properties as those of a passive solution, while it is totally reasonable to expect the properties of the tube to be changed by activity. Another assumption that should be tested is the one that the active fluctuations couple only to the longitudinal modes.

Much more work is needed to understand the nature of the spatially inhomogeneous state [29–31]. We have not included motor transport in the above description, which is important for very processive motors and at low motor densities. It will also be interesting to study the effect of shear flow on the formation and stability of spatially inhomogeneous structures.

Acknowledgments

This work has been done in collaboration with A C Maggs, A Ajdari and M C Marchetti. I thank E Frey, F Jülicher, K Kruse, F MacKintosh, D Morse, S Ramaswamy, M Rao and R A Simha for helpful discussions. This research was supported in part by the National Science Foundation under Grants PHY99-07949 (at KITP) and DMR97-30678 (at Syracuse), and the Royal Society.

References

[1] Howard J 2000 *Mechanics of Motor Proteins and the Cytoskeleton* (New York: Sinauer)
[2] Dogterom M, Maggs A C and Leibler S 1995 *Proc. Natl Acad. Sci. USA* **92** 6683
[3] Takiguchi K 1991 *J. Biochem.* **109** 520
Urrutia R *et al* 1991 *Proc. Natl Acad. Sci.* **88** 6701
[4] Nédélec F J, Surrey T, Maggs A C and Leibler S 1997 *Nature* **389** 305
[5] Surrey T, Nédélec F J, Leibler S and Karsenti E 2001 *Science* **292** 1167
[6] Humphrey D, Duggan C, Saha D, Smith D and Käs J 2002 *Nature* **416** 413
[7] Nedelec F 1998 *PhD Thesis* Université Paris XI
[8] Nakazawa H and Sekimoto K 1996 *J. Phys. Soc. Japan* **65** 2404
Sekimoto K and Nakazawa H 1998 *Current Topics in Physics* ed Y M Cho, J B Homg and C N Yang (Singapore: World Scientific)
[9] Kruse K and Jülicher F 2000 *Phys. Rev. Lett.* **85** 1778
Kruse K and Jülicher F 2003 *Phys. Rev.* E **67** 051913
[10] Liverpool T B, Maggs A C and Ajdari A 2001 *Phys. Rev. Lett.* **86** 4171
[11] Liverpool T B and Marchetti M C 2003 *Phys. Rev. Lett.* **90** 138102
[12] Liverpool T B and Marchetti M C 2004 *Preprint* cond-mat/0406276
[13] Prost J 2000 unpublished

[14] Doi M and Edwards S F 1992 *The Theory of Polymer Dynamics* (Oxford: Clarendon)
[15] Langer S A and Liu A J 2000 *Europhys. Lett.* **49** 68
[16] Odijk T 1983 *Macromolecules* **16** 1340
[17] Doi M 1985 *J. Polym. Sci.: Polym. Symp.* **73** 93
[18] Semenov A N 1986 *J. Chem. Soc., Faraday Trans.* **2** 317
[19] Isambert H and Maggs A C 1996 *Macromolecules* **29** 1036
[20] MacKintosh F C, Käs J and Janmey P A 1995 *Phys. Rev. Lett.* **75** 4425
[21] Maggs A C 1998 *Phys. Rev.* E **57** 2091
[22] Morse D C 1998 *Phys. Rev.* E **58** R1237
Morse D C 1998 *Macromolecules* **31** 7030
Morse D C 1998 *Macromolecules* **31** 7044
[23] Gittes F and MacKintosh F C 1998 *Phys. Rev.* E **58** R1241
[24] Everaers R *et al* 1999 *Phys. Rev. Lett.* **82** 3717
[25] Liverpool T B and Maggs A C 2001 *Macromolecules* **34** 6064–73
Shankar V, Pasquali M and Morse D C 2002 *J. Rheol.* **46** 1111
[26] Bassetti B, Lagomarsino M C and Jona P 2000 *Eur. Phys. J.* B **15** 483
[27] Lee H Y and Kardar M 2001 *Phys. Rev.* E **64** 56113
Kim J *et al* 2003 *J. Korean Phys. Soc.* **42** 163
[28] Kruse K and Sekimoto K 2002 *Phys. Rev.* E **66** 031904
Parmeggiani A *et al* 2003 *Phys. Rev. Lett.* **90** 086601
[29] Kruse K *et al* 2003 *Europhys. Lett.* **64** 716
[30] Kruse K *et al* 2004 *Phys. Rev. Lett.* **92** 078101
[31] Simha R A and Ramaswamy S 2002 *Phys. Rev. Lett.* **89** 058101
Hatwalne Y *et al* 2004 *Phys. Rev. Lett.* **92** 118101
[32] Sankaraman S, Menon G I and Sunil Kumar P B 2003 *Preprint* cond-mat/0311540
[33] Kruse K, Camalet S and Jülicher F 2001 *Phys. Rev. Lett.* **87** 138101
[34] Teraoka I and Hayakawa R 1988 *J. Chem. Phys.* **89** 6989
Teraoka I and Hayakawa R 1989 *J. Chem. Phys.* **91** 2643